Voltage Sensorless Based Model Predictive Control With Battery Management System: For Solar PV Powered On-Board EV Charging

Nishant Kumar, *Senior Member, IEEE*, Bhim Singh, *Fellow, IEEE*, and Bijaya Ketan Panigrahi, *Senior Member, IEEE*

***Abstract*— This work deals with a novel voltage sensorless based model predictive control (VSPC) scheme for continuous and quick maximum power harvesting (MPH) from a photovoltaic (PV) array for a solar-powered on-board electric vehicle (EV) charging system. In VSPC, the first model predictive control (MPC) is used with a PV array to predict the system state in the horizon of time and to eliminate the voltage sensor. An adaptive concept is used for deciding the operating point, which accelerates the tracking process and improves dynamic performance during irradiation changes and shading pattern changes in partially shaded conditions. Moreover, VSPC also takes care of the EV charging process using the EV-provided battery management system (BMS) command or threshold safety limits of the EV battery. The working principle of VSPC is based on a prediction of the future behavior of the system. It realizes on a selected time horizon, in an arbitrary number of samples, which is decided according to the complexity of the fitness function. In order to minimize or maximize the fitness function, it predicts the voltage of the solar PV array as well as tunes the present control signal, which forces it to converge or reach the convergence criteria. Moreover, the cost and response time of current sensors are lower than voltage sensors. Therefore, the VSPC control gives a fast response and low power oscillations in steady-state compared to conventional techniques. This control technique is verified on a developed prototype of the PV system in different shading and irradiance conditions, as well as the system stability, is analyzed through the Bode plot. The system performance is also compared with the state-of-the-art methods.**

***Index Terms*— Battery management system (BMS), electric vehicle (EV), maximum power point tracking (MPPT), model predictive control (MPC), partial shading condition, photovoltaic (PV), solar powered EV (SP-EV), voltage sensor-less.**

I. Introduction

NOWADAYS, the application of solar photovoltaic (PV) power has grown substantially. On low power ratings in residential areas and high power ratings in commercial levels, as well as in aerospace equipment, solar PV arrays are used very frequently [1]. Moreover, to avoid fossil fuel, solar-powered electric vehicle (SP-EV) is used. In each system, the user wants to harvest maximum and quality power from the PV panel. Here the meaning of quality is oscillations-free power in the steady-state and quick response during dynamic conditions, which is only possible through a strong maximum power harvesting (MPH) technique.

For MPH, one needs a global maximum power point tracking (GMPPT) algorithm. Because the power–voltage or power–current characteristic of the PV array consists of a nonlinear nature [2], [3]. Therefore, the maximum power exists, only on a single voltage and a single current on PV characteristics [4]. An exhaustive literature survey reveals that for GMPPT, several techniques have been proposed such as hill-climbing [5], perturb and observe (P&O) [6], and incremental conductance (InC) [7]. However, according to the situation, these techniques are unable to decide an optimal step size. Therefore, these techniques are suffered from steady-state oscillation and longer tracking duration issues. Because, a small step size gives a good steady-state performance, while it takes a longer time to reach the maximum power peak (MPP) during the dynamic condition. Similarly, a large step size gives a good dynamic performance, while during the steady-state condition, it creates oscillations in the output. Moreover, during sudden and large irradiation fall conditions, these techniques lose the tracking direction. A few techniques have been proposed to solve these issues, such as modified P&O (MP&O) [8], modified InC, improved P&O [9], improved InC, etc. However, no one algorithm is perfect for all types of situations. Few techniques have oscillation-free steady-state performance, but the performances are very poor during dynamic conditions. Some algorithms have good tracking capability in a dynamic condition, but during a steady-state condition produce oscillation in the output. Some of them have an optimal solution for both steady-state and dynamic conditions. However, computational burden and large design dependences are the main constraint.

Some other techniques, like fractional open circuit voltage and short circuit current, are also famous, where step size depends on panel ratings, such as open-circuit voltage and short circuit current of the solar PV panel. However, in the entire life of the PV panel, the ratings are not constant. Therefore, these techniques are not reliable solutions for maximum power point tracking (MPPT). Moreover, some researchers have proposed, improved model-based MPPT [10], current control loop-based MPPT [11], closed-loop MPPT [12], discrete current sensing-based MPPT [13], root-finding techniques-based MPPT, incremental resistance-based MPPT, sliding mode MPPT, and MPPT based on ripple correlation. However, improvements in solutions are not remarkable and significant because these techniques perform

Manuscript received 15 March 2022; revised 30 April 2022, 9 July 2022, and 29 September 2022; accepted 6 October 2022. Date of publication 10 October 2022; date of current version 13 June 2023. This work was supported by the Science and Engineering Research Board (SERB), Government of India-National Science Chair (NSC) Fellowship. *(Corresponding author: Nishant Kumar.)*

Nishant Kumar is with the Electrical Engineering Department, IIT Jodhpur, Jodhpur 342011, India (e-mail: nishantkumar@iitj.ac.in).

Bhim Singh and Bijaya Ketan Panigrahi are with the Electrical Engineering Department, IIT Delhi, New Delhi 110016, India.

Digital Object Identifier 10.1109/TTE.2022.3213253

very well during a few irradiation patterns. While, during other types of irradiation patterns, these techniques cannot find the optimal solution. After these, artificial intelligence techniques, such as fuzzy logic [14], neural networks, etc., have been used for MPPT [15]. However, fuzzification and training require huge amounts of data, which creates computational burden and complexity, so these techniques are not popular. Some researchers have proposed soft computing-based techniques for MPPT, such as particle swarm optimization (PSO) [16], firefly optimization, differential evolution, whale optimization with differential evolution (WODE) [17], harmony search, etc. However, the problems with these techniques are the same as artificial intelligence-based algorithms. For searching, it requires a big population of searching agents, which creates a huge computational burden and poor dynamic performance.

A substantial literature shows that after these techniques, researchers have tried model predictive control (MPC) based MPPT such as multi-sensor based MPC MPPT [18]. This technique [18] is shown excellent performance in different solar irradiance conditions. However, it is based on three sensors (two-voltage sensors and one-current sensor), which is not an economical solution. Moreover, extremum-seeking-based MPC MPPT [19] and modified MPC MPPT [20] algorithms have been proposed. These techniques have needed one sensor by using an output observer, such as extremum seeking-based MPC MPPT [19] is based on a one-voltage sensor, one-current sensor, and one-output current observer, and modified MPC MPPT [20] is based on a one-voltage sensor, one-current sensor, and one-output voltage observer. However, designing an accurate observer according to the system is the key challenge in these techniques. Somehow these issues are tried to solve in [21], [22], and [23]. However, it is limited to a resistive load. In the case of EV or battery charging, charging current monitoring or battery management system (BMS) requires for safe operation.

A. Motivation

The major problems with these all techniques are that all techniques require two sensors, one voltage, and one current sensor [24]. The limitations of this type of technique are that it monitors only input terminal parameters, as well as the solar voltage is less sensitive to the change in solar irradiance and environmental temperature, which makes dynamic response slower. Moreover, the cost and response time of voltage sensors are higher and poor than current sensors. Therefore, researchers have concentrated on voltage-sensorless MPPT techniques. The available literature reveals that the Cauchy and Gaussian sine cosine optimization algorithm [25] and MPC [21], [22], [23] based techniques have been used available for MPPT only by using the current sensor. However, the major limitation of this technique is that it is only applicable to batteries [25] and resistive loads [21], [22], [23]. These are not applicable for EV with BMS support. Moreover, it is based on population-based searching, which creates a huge computational burden. Therefore, it is not possible to implement on a low-cost microprocessor [26], [27], [28], [29], [30], [31], [32], [33], [34]. These issues motivate a generalized current sensor-based MPPT algorithm. Therefore, a novel voltage sensorless-based model predictive control (VSPC) scheme is developed for SP-EV applications to operate with the partially shaded conditions for EV charging applications, which have continuous, quick, and better dynamic performers during MPH from the solar PV panel.

II. Voltage Sensor-Less Predictive Control

The general principle of the MPH is based on the output of one voltage and one current sensor, which decides the PV power. However, the voltage is less sensitive to the change in solar irradiance and environmental temperature. Moreover, the cost and response time of voltage sensors are higher and poor than current sensors. Therefore, for the elimination of the voltage sensor, the model predictive control (MPC) is used here, as well as it also reduces the ripples in output power. Moreover, adaptive control is used here to improve the system's dynamic response.

A. Model Predictive Control

The working principle of MPC [26] is based on a prediction of the future behavior of the system. It realizes on a selected time horizon, in an arbitrary number of samples, which is decided according to the complexity of the fitness function [27]. In order to minimize or maximize the fitness function, it predicts the future steps as well as tunes the present control signal, which forces it to converge or reach the convergence criteria. The future response is denoted as, $\tilde{S}(n+N)$, where $N=1$.

The fitness function (ff) is described as

$$\text{ff} = \min(f(S(n), u(n), \ldots, u(n+N-1))) \tag{1}$$

where L is the time horizon, $u(n)$ is the controller output. The controller output is totally dependent on the switching ON ($\xi = 1$)/OFF ($\xi = 0$) state.

In an optimization problem, at each sampling time, the problem is solved by using sensed variables ($S(n)$), and it predicts the future response ($\tilde{S}(n+N)$) by using MPC at different switching states ($\xi \in [1{:}\ x]$), where x is the total number of states. After that, the predicted results are compared with the reference response, and it generates an error. Then the new objective is to minimize the error signal, which helps fulfill the expected response. The objective function and constraints are described as [26]

$$\varepsilon = \min \begin{pmatrix} \mu_1 \left| \tilde{S}_1^{\xi \in [1:x]}(n+1) - S_1^*(n+1) \right| \\ +\mu_2 \left| \tilde{S}_2^{\xi \in [1:x]}(n+1) - S_2^*(n+1) \right| \\ \ldots\ldots + \mu_I \left| \tilde{S}_I^{\xi \in [1:x]}(n+1) - S_I^*(n+1) \right| \end{pmatrix} \tag{2}$$

$$S(n) \leq S_{\text{Limit}} \tag{3}$$

where μ is the weight factor or importance factor of each objective. S_{Limit} is the maximum value of the variable. The flowchart of the MPC is given in Fig. 1.

B. Voltage Sensorless Predictive Control

In VSPC, two current sensors are used, one close to the PV panel, which senses the PV current, and one sensor close to the load, which senses the load current. Here, by using these two currents, MPC decides the PV voltage and predicts the PV current for the next sampling time. It is described in two

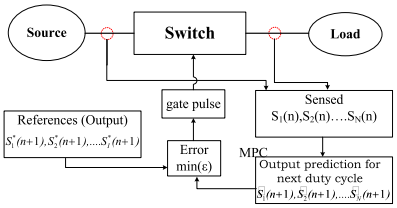

Fig. 1. Flowchart of optimization by using MPC.

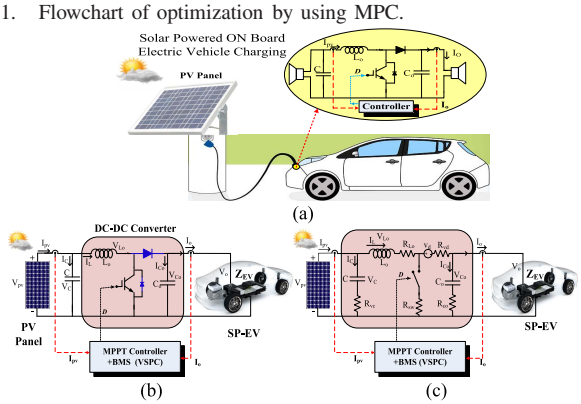

Fig. 2. SP-EV charging. (a) Working model, (b) circuit network, and (c) detailed circuit network with component losses.

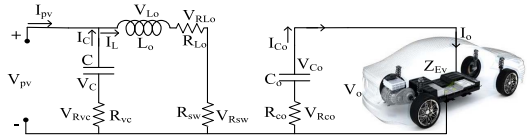

Fig. 3. Circuit configuration when switch is ON.

states (ON and OFF). The complete working of the PV array with a boost converter, load, and sensors is shown in Fig. 2.

Here, $V_{\rm pv}$ and $I_{\rm pv}$ are PV voltage and current. I_o and V_o are load voltage and current. $Z_{\rm EV}$ is the equivalent impedance of EV. L_o is an interfacing inductor, the voltage across and current through L_o are denoted as $V_{\rm Lo}$ and I_L. The voltage across and current through the capacitor (C_o) of the output filter are denoted as $V_{\rm Co}$ and $I_{\rm Co}$. Moreover, V_C and I_C are the voltage and current of the energy-storing capacitor (C). The sampling instant is N_s (index is n) and D represents the duty cycle of the boost converter. $R_{\rm VC}$, $R_{\rm LO}$, $R_{\rm sw}$, and $R_{\rm CO}$ are series resistance of $C_{\rm VC}$, L_O, switch, and C_O, respectively, to represent the power loss of each component. $R_{\rm vd}$ and V_d are diode dynamic resistance and forward voltage.

1) When the switch is ON ($\xi = 1$), the circuit is shown in Fig. 3.
Using nodal analysis, the obtained relations are as follows:

$$V_{\rm PV} = V_C + V_{\rm Rvc} \tag{4}$$

$$\left.\begin{aligned} I_{\rm pv}(n) + I_c(n) &= I_L(n) \\ I_C(n) &= C\frac{dV_C(n)}{dn} = \frac{V_{\rm Rvc}}{R_{\rm vc}} \end{aligned}\right\} \tag{5}$$

$$I_o(n) = I_{\rm co}(n),\ V_o(n) = V_{\rm co}(n) + V_{\rm Rco}(n)\} \tag{6}$$

$$\left.\begin{aligned} I_o(n)Z_{\rm EV} &= V_{\rm Co}(n) + V_{\rm Rco}(n) \\ I_o(n)Z_{\rm EV} &= \frac{1}{C_o}\int I_o(n)dn + I_o(n)R_{\rm co} \end{aligned}\right\}. \tag{7}$$

The discretization of (7), by using the trapezoidal approximation method is as follows [31]:

$$\left.\begin{aligned} I_o(n)Z_{\rm EV} &= \frac{N_s}{C_o}\left(\frac{I_o(n)+I_o(n+1)}{2}\right) + I_o(n)R_{\rm Co} \\ I_o(n+1) &= \frac{\{2C_o(Z_{\rm EV}-R_{\rm Co})-N_s\}}{N_s}I_o(n) \end{aligned}\right\}. \tag{8}$$

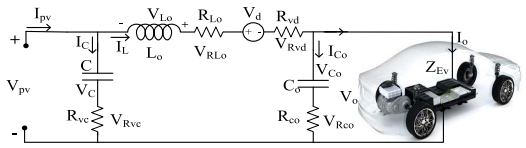

Fig. 4. Circuit configuration when switch is OFF.

a) The predicted PV current ($\tilde{I}_{\rm pv}^{\xi=1}(n+1)$) for the boost converter at sampling time ($n+1$), during switch ON is as

$$\tilde{I}_{\rm pv}^{\xi=1}(n+1) = \frac{1}{1-D}\left[\frac{\{2C_o(Z_{\rm EV}-R_{\rm Co})-N_s\}}{N_s}\right]I_o(n). \tag{9}$$

2) When the switch is OFF ($\xi = 0$), the circuit is shown in Fig. 4.
Using nodal analysis, the obtained relations are as

$$\left.\begin{aligned} I_L(n) &= I_o(n) + I_{\rm co}(n) \\ I_{\rm pv}(n) &= I_L(n) + I_c(n) \end{aligned}\right\} \tag{10}$$

$$\left.\begin{aligned} V_o(n) &= V_{\rm Co}(n) + V_{\rm Rco}(n) \\ I_o(n)Z_{\rm EV} &= \frac{1}{C_o}\int I_{\rm Co}(n)dn + I_{\rm Co}(n)R_{\rm Co} \end{aligned}\right\}. \tag{11}$$

Discretization of (11), using the trapezoidal approximation method [28] is described as follows:

$$\left.\begin{aligned} I_o(n)Z_{\rm EV} &= \frac{N_s}{C_o}\left(\frac{I_{\rm Co}(n)+I_{\rm Co}(n+1)}{2}\right) + I_{\rm Co}(n)R_{\rm Co} \\ I_{\rm Co}(n+1) &= I_o(n)\frac{2C_oZ_{\rm EV}}{N_s} - I_{\rm Co}(n)\left(1+\frac{2C_oR_{\rm Co}}{N_s}\right) \end{aligned}\right\}. \tag{12}$$

From (10) and (11), the average PV voltage is as

$$\left.\begin{aligned} V_{\rm pv}(n) &= V_C + V_{\rm Rvc},\ V_{\rm pv}(n) \\ &= \frac{1}{C}\int I_C(n)dn + I_C(n)R_{\rm vc} \\ V_{\rm pv}(n) &= \frac{1}{C}\int\left(I_{\rm pv}(n) - I_O(n) - I_{\rm CO}(n)\right)dn \\ &\quad +\left(I_{\rm pv}(n) - I_O(n) - I_{\rm CO}(n)\right)R_{\rm vc} \end{aligned}\right\}. \tag{13}$$

Discretization of (13), using the trapezoidal approximation method is described as follows:

$$\left.\begin{aligned} V_{\rm pv}(n) &= \frac{1}{C}\int\left(I_{\rm pv}(n) - I_O(n) - I_{\rm CO}(n)\right)dn \\ &\quad +\left(I_{\rm pv}(n) - I_O(n) - I_{\rm CO}(n)\right)R_{\rm vc} \\ V_{\rm pv}(n) &= \left(\frac{N_s}{2C} + R_{\rm vc}\right)\left(I_{\rm pv}(n) - I_O(n) - I_{\rm CO}(n)\right) \\ &\quad +\frac{N_s}{2C}\left(I_{\rm pv}(n+1) - I_O(n+1) - I_{\rm CO}(n+1)\right) \end{aligned}\right\}. \tag{14}$$

$V_{\rm pv}$ is also derived as

$$\left.\begin{aligned} V_{\rm pv}(n) &= -V_{\rm Lo}(n) + V_{RLo}(n) \\ &\quad +V_d + V_{Rvd}(n) + V_o(n) \\ V_{\rm pv}(n) &= -L_o\frac{dI_L(n)}{dn} + I_L(n)(R_{\rm Lo}+R_{\rm vd}) \\ &\quad +V_d + I_o(n)Z_{\rm Ev} \end{aligned}\right\} \tag{15}$$

$$V_{\rm pv}(n) = \begin{pmatrix} -L_o\frac{d(I_o(n)+I_{\rm co}(n))}{dn} \\ +(I_o(n)+I_{\rm co}(n)) \\ \times(R_{\rm Lo}+R_{\rm vd}) + V_d + I_o(n)Z_{\rm Ev} \end{pmatrix}. \tag{16}$$

Discretization of (16), using the Euler approximation method is described as follows:

$$V_{\rm pv}(n) = \frac{-L_o}{N_s}I_o(n+1) + \left(R_{\rm Lo}+R_{\rm vd}+Z_{\rm Ev}+\frac{L_o}{N_s}\right)I_o(n) - \frac{L_o}{N_s}I_{\rm Co}(n+1) + \left(R_{\rm Lo}+R_{\rm vd}+\frac{L_o}{N_s}\right)I_{\rm Co}(n) + V_d. \tag{17}$$

From (12), (14), and (17), $I_{\mathrm{Co}}(n)$ is derived as

$$I_o(n+1)=\frac{1}{\begin{pmatrix}-\frac{L_o}{N_s}\\+\frac{N_s}{2C}\end{pmatrix}}\times\begin{bmatrix}\left(\frac{N_s}{2C}+R_{\mathrm{vc}}\right)I_{\mathrm{pv}}(n)+\frac{N_s}{2C}I_{\mathrm{pv}}(n+1)\\-I_{\mathrm{Co}}(n)\begin{pmatrix}R_{\mathrm{Lo}}+R_{\mathrm{vd}}+R_{\mathrm{vc}}\\+\frac{2L_o}{N_s}+\frac{2C_oR_{\mathrm{Co}}L_o}{N_s^2}-\frac{C_oR_{\mathrm{Co}}}{C}\end{pmatrix}-V_d\\-\begin{pmatrix}R_{\mathrm{Lo}}+R_{\mathrm{vd}}+Z_{\mathrm{Ev}}+\frac{N_s}{2C}+R_{\mathrm{vc}}\\+\frac{L_o}{N_s}-\frac{2C_oZ_{\mathrm{EV}}L_o}{N_s^2}+\frac{C_oZ_{\mathrm{EV}}}{C}\end{pmatrix}I_o(n)\end{bmatrix} \tag{18}$$

b) The predicted PV current ($\tilde{I}_{\mathrm{pv}}^{\xi=0}(n+1)$) for the boost converter at sampling time ($n+1$), during switch OFF is

$$\tilde{I}_{\mathrm{pv}}^{\xi=0}(n+1)=\frac{1/(1-D)}{\begin{pmatrix}-\frac{L_o}{N_s}\\+\frac{N_s}{2C}\end{pmatrix}}\times\begin{bmatrix}\left(\frac{N_s}{2C}+R_{\mathrm{vc}}\right)I_{\mathrm{pv}}(n)+\frac{N_s}{2C}I_{\mathrm{pv}}(n+1)-I_{\mathrm{Co}}(n)\\\times\begin{pmatrix}R_{\mathrm{Lo}}+R_{\mathrm{vd}}+R_{\mathrm{vc}}\\+\frac{2L_o}{N_s}+\frac{2C_oR_{\mathrm{Co}}L_o}{N_s^2}-\frac{C_oR_{\mathrm{Co}}}{C}\end{pmatrix}-V_d\\-\begin{pmatrix}R_{\mathrm{Lo}}+R_{\mathrm{vd}}+Z_{\mathrm{Ev}}+\frac{N_s}{2C}+R_{\mathrm{vc}}\\+\frac{L_o}{N_s}-\frac{2C_oZ_{\mathrm{EV}}L_o}{N_s^2}+\frac{C_oZ_{\mathrm{EV}}}{C}\end{pmatrix}I_o(n)\end{bmatrix} \tag{19}$$

$$\tilde{I}_{\mathrm{pv}}^{\xi=0}(n+1)=\frac{2CN_s}{\begin{pmatrix}2CL_o\times\\(D-1)\\-DN_s^2\end{pmatrix}}\times\begin{bmatrix}\left(\frac{N_s}{2C}+R_{\mathrm{vc}}\right)I_{\mathrm{pv}}(n)\\-I_{\mathrm{Co}}(n)\begin{pmatrix}R_{\mathrm{Lo}}+R_{\mathrm{vd}}+R_{\mathrm{vc}}\\+\frac{2L_o}{N_s}+\frac{2C_oR_{\mathrm{Co}}L_o}{N_s^2}-\frac{C_oR_{\mathrm{Co}}}{C}\end{pmatrix}\\-V_d-\begin{pmatrix}R_{\mathrm{Lo}}+R_{\mathrm{vd}}+Z_{\mathrm{Ev}}+\frac{N_s}{2C}+R_{\mathrm{vc}}\\+\frac{L_o}{N_s}-\frac{2C_oZ_{\mathrm{EV}}L_o}{N_s^2}+\frac{C_oZ_{\mathrm{EV}}}{C}\end{pmatrix}I_o(n)\end{bmatrix} \tag{20}$$

These predictions generate a reference current ($\underset{\sim}{I}_{\mathrm{pv}}^{*}(n)$) through adaptive control and MPH algorithm.

C. Adaptive Control

The responsibility of the adaptive control is to generate a suitable set of duty cycles, $D^k(n+1)$, and reference currents ($\underset{\sim}{I}_{\mathrm{pv}}^{*,k}(n)$) for jj number of populations. This selection is based on an adaptive control technique to manage the current position on the power–current characteristic, which is decided through the slope. If the slope is positive, it means to need an increase the current for MPH, so a decrease the duty cycle. Similarly, if the slope is negative, it means to need a decrease the current for MPH, so an increase the duty cycle. The amount of increment and decrement in the duty cycle is decided according to the error factor (α^k) and the power mismatch factor (β^k). Moreover, the reference current is generated using Lagrange polynomial interpolation [25], based on the power mismatch factor updated duty cycle. The β is defined as

$$\beta^k=\frac{\left|\Delta P^k(n)-\Delta P^k(n-1)\right|}{\left|P^k(n)-P^k(n-1)\right|}\times\frac{\left|D^k(n)-D^k(n-1)\right|}{\left|\Delta D^k(n)-\Delta D^k(n-1)\right|}\quad k=1,2,\ldots,jj \tag{21}$$

where $\Delta P^k(n)$ and $\Delta P^k(n-1)$ are the changes in power for the kth searching agent at nth and $n-1$th time instants. $P^k(n)$ and $P^k(n-1)$ are the powers for the kth searching agent at nth and $n-1$th time instants. $\Delta D^k(n)$ and $\Delta D^k(n-1)$ are the changes in duty cycles for the kth searching agent at nth and $n-1$th time instants. $D^k(n)$ and $D^k(n-1)$ are duty cycles for the kth searching agent at nth and $n-1$th time instants. $I^k(n)$ and $I^k(n-1)$ are current for kth searching agents at nth and $n-1$th time instants.

The addition or subtraction in the duty cycle is according to the slope. The sign of the slope (λ^k) is defined as

$$\text{if; }\frac{P^k(n)-P^k(n-1)}{I^k(n)-I^k(n-1)}>0\begin{cases}\text{if; } I^k(n)-I^k(n-1)>0\\\Rightarrow\lambda^k=-1\\\text{Else }\Rightarrow\lambda^k=+1\end{cases},\quad\text{Else}\begin{cases}\text{if; } I^k(n)-Iv(n-1)>0\\\Rightarrow\lambda^k=+1\\\text{Else}\Rightarrow\lambda^k=-1\end{cases}\quad k=1,2,\ldots,jj \tag{22}$$

β^k based on updated duty cycles are as

$$D^{\beta,k}(n+1)=D^k(n)+\lambda^k\times\beta^k;\quad k=1,2,\ldots,jj. \tag{23}$$

1) The reference current ($\underset{\sim}{I}_{\mathrm{pv}}^{*,k}(n)$) is generated as (24), shown at the bottom of the next page.
The α is defined as

$$\alpha^k=\frac{\left|\underset{\sim}{I}_{\mathrm{pv}}^{*,k}(n)-\tilde{I}_{\mathrm{pv}}^{k,\xi\in[0,1]}(n+1)\right|}{\underset{\sim}{I}_{\mathrm{pv}}^{*,k}(n)},\quad k=1,2,\ldots,jj. \tag{25}$$

Therefore, the change in the duty cycle is defined as

$$\Delta D^k(n+1)=\alpha^k+\beta^k,\quad k=1,2,\ldots,jj. \tag{26}$$

2) The updated duty cycle is as

$$D^k(n+1)=D^k(n)+\lambda^k\times\Delta D^k(n+1),\quad k=1,2,\ldots,.jj. \tag{27}$$

This process is repeated jj times, where jj is the number of searching agents. Therefore, a set of updated duty cycles generates.

These duty cycles are the key to MPH, which quickly responds during dynamic conditions and gives ripple-free output power in steady-state conditions.

D. Applications of VSPC

In VSPC, for $D^k(n+1)$, by sensing I_{pv}^k and I_o^k, it predicts $V_{\mathrm{pv}}^k(n)$ and $\tilde{I}_{\mathrm{pv}}^{k,\xi=1}(n+1)$ of the next step by using MPC. Moreover, through adaptive control, $\underset{\sim}{I}_{\mathrm{pv}}^{*,k}(n)$ and $\Delta D^k(n+1)$ are calculated, which maximizes the output power and minimizes the fitness function.

1) The fitness function (ϕ) is described as

$$\phi=\min\left[\left|\tilde{I}_{\mathrm{pv}}^{k,\xi\in[0,1]}(n+1)-\underset{\sim}{I}_{\mathrm{pv}}^{*,k}(n)\right|\right],\quad k=1,2,\ldots,jj. \tag{28}$$

This minimization drives the searching in a steady-state condition. To sense the dynamic condition, the power envelop concept is used. The envelop limit is $\delta\delta$ (~1% of

PV panel power rating) is used. The condition detection using the power envelop concept is described as follows:

$$\xi\xi = \max\left[|\Delta P^k(n)|\right], \quad k = 1, 2, \ldots, jj \tag{29}$$

$$\text{if } \xi\xi \le \delta\delta \Rightarrow \text{Steady-state Condition}$$

$$\text{else } \xi\xi > \delta\delta \Rightarrow \text{Dynamic Condition.} \tag{30}$$

During the dynamic condition, VSPC stops conversance and expands the searching area. Moreover, in a steady-state condition, VSPC continues conversance and moves toward the true global power point.

E. BMS of VSPC

In VSPC, during EV charging, the first priority is to follow the vehicle-based "BMS" command. This BMS command provides the maximum optimal and safe charging current reference (ξ_{BMS}). Therefore, VSPC is to maintain a charging current equal to ξ_{BMS}. Otherwise, VSPC tries to maintain the charging current above the lower EV charging current threshold limit (ξ_{EVL}). Therefore, in the case of a BMS regulated system, the charging current is to be in between [ξ_{EVL}, ξ_{BMS}]. This control action is described as follows:

$$\left.\begin{array}{l} \text{if } I_{\text{EV}}(n) \ge \xi_{\text{BMS}} \Rightarrow I_o(n) = \xi_{\text{BMS}} \\ \text{else if } I_{\text{EV}}(n) < \xi_{\text{EVL}} \Rightarrow I_o(n) = 0 \\ \text{else } I_o(n) = I_{\text{EV}}(n) \end{array}\right\}. \tag{31}$$

However, if vehicle-based BMS is not available, then VSPC keeps the charging current in between the lower EV charging current threshold limit (ξ_{EVL}), and a higher EV charging current threshold limit (ξ_{EVH}).

In case, available solar power is not sufficient to maintain the ξ_{EVL}, then changing process is to be stopped. This scheme is described as follows:

$$\left.\begin{array}{l} \text{if } I_{\text{EV}}(n) \ge \xi_{EVH} \Rightarrow I_o(n) = \xi_{EVH} \\ \text{else if } I_{\text{EV}}(n) < \xi_{\text{EVL}} \Rightarrow I_o(n) = 0 \\ \text{else } I_o(n) = I_{\text{EV}}(n) \end{array}\right\}. \tag{32}$$

The flowchart of the VSPC algorithm is shown in Fig. 5.

III. Results and Discussion

The performance of the VSPC-based MPPT algorithm is evaluated in different types of irradiations and shading changing conditions, such as uniform shading conditions, and in partially shaded conditions. Moreover, to validate the effectiveness of VSPC based MPPT algorithm, the obtained performances are compared with the performances of the most popular state-of-the-art techniques, such as P&O and hybrid P&O with PSO (P&O-PSO).

For experimentation, a prototype of the system is developed for performance evaluation of this VSPC MPPT technique for SP-EV system, which is illustrated in Fig. 6. To realize the PV characteristic, a solar PV simulator (AMETEK, ETS600 $\times$ 17DPVF) is used, and for MPPT dc–dc boost converter is used. A DSpace (Digital Signal Processor for Applied and Control Engineering) controller (1202-DSPACE) is used for the execution of control techniques. A digital storage oscilloscope (DSO7014A) is used for dynamic performance analysis. During implementation, the required catch memory and RAM on the processor are 5 MB and 1 GB, respectively. Hall-effect current (LA-55p) and voltage (LV-25) sensors are used for sensing all signals. Here, to remove high di/dt issues, the output of current sensor is crossed through and "spike removal notch filter" and "moving average" calculation logics to decide the actual, noise-free, and ripple free current information for rest of the calculation.

A. Uniform Shading Condition on Solar PV Panel

The irradiation pattern for uniform shading conditions is illustrated in Fig. 7(a). During experimentation, the considered data of the circuit are, $V_{\text{oc}} = 120$ V, $I_{\text{sc}} = 2$ A, $V_{\text{EV}} = 140$ V, $V_{\text{mpp}} = 103.3412$ V, $I_{\text{mpp}} = 1.8962$ A, and $P_{\text{mpp}} = 195.9312$ W. For clear visibility, the test results are shown in two parts, first sudden irradiation rises from 800 to 1000 W/m^2, and in the second case, sudden irradiation falls from 1000 to 800 W/m^2. The obtained results of VSPC, P&O, and P&O-PSO techniques for sudden irradiation rise and fall conditions are illustrated in Figs. 7(d), (c), and (b) and 8(c), (b), and (a), respectively. In each result, obtained PV current (I_{PV}), PV voltage (V_{PV}), PV power (P_{PV}), and duty cycle (D) are given. Here, $\xi_{\text{EVL}} = 0.5$ A, and $\xi_{\text{EVH}} = 2.5$ A are considered. At 800 and 1000 W/m^2 solar irradiance, I_{EV} is 1.12 and 1.4 A, respectively, which is in between ξ_{EVL} and ξ_{EVH}. Therefore, the BMS of VSPC allows it to operate at MPP and charge EV with the maximum possible current.

Figs. 7 and 8 reveal that, for uniform shading conditions, each algorithm has MPP tracking capability. However, during the dynamics condition, the deviation from the actual track is recorded in the case of the P&O technique, as well as the oscillation in the waveform is also very high. In the P&O-PSO algorithm, researchers have tried to solve the deviation problem, and deviation during insolation rise condition is successfully mitigated. However, deviation during the insolation fall condition and oscillation in the steady-state condition is still in the output waveforms. In Figs. 7(b) and 8(a), the waveforms of the duty cycle, show that these algorithms are suffered from longer tracking duration and direction deviation problems,

$$\underset{\sim}{I}^{*,k}_{\text{pv}}(n) = \left[\begin{array}{l} \dfrac{\left(D^{\beta,k}(n+1) - D^k(n-1)\right)\left(D^{\beta,k}(n+1) - D^k(n-2)\right)\left(D^{\beta,k}(n+1) - D^k(n-3)\right) \times I^k_{\text{pv}}(n)}{\left(D^k(n) - D^k(n-1)\right)\left(D^k(n) - D^k(n-2)\right)\left(D^k(n) - D^k(n-3)\right)} \\ + \dfrac{\left(D^{\beta,k}(n+1) - D^k(n)\right)\left(D^{\beta,k}(n+1) - D^k(n-2)\right)\left(D^{\beta,k}(n+1) - D^k(n-3)\right) \times I^k_{\text{pv}}(n-1)}{\left(D^k(n-1) - D^k(n)\right)\left(D^k(n-1) - D^k(n-2)\right)\left(D^k(n-1) - D^k(n-3)\right)} \\ + \dfrac{\left(D^{\beta,k}(n+1) - D^k(n)\right)\left(D^{\beta,k}(n+1) - D^k(n-1)\right)\left(D^{\beta,k}(n+1) - D^k(n-3)\right) \times I^k_{\text{pv}}(n-2)}{\left(D^k(n-2) - D^k(n)\right)\left(D^k(n-2) - D^k(n-1)\right)\left(D^k(n-2) - D^k(n-3)\right)} \\ + \dfrac{\left(D^{\beta,k}(n+1) - D^k(n)\right)\left(D^{\beta,k}(n+1) - D^k(n-1)\right)\left(D^{\beta,k}(n+1) - D^k(n-2)\right) \times I^k_{\text{pv}}(n-3)}{\left(D^k(n-3) - D^k(n)\right)\left(D^k(n-3) - D^k(n-1)\right)\left(D^k(n-3) - D^k(n-2)\right)} \end{array}\right] \tag{24}$$

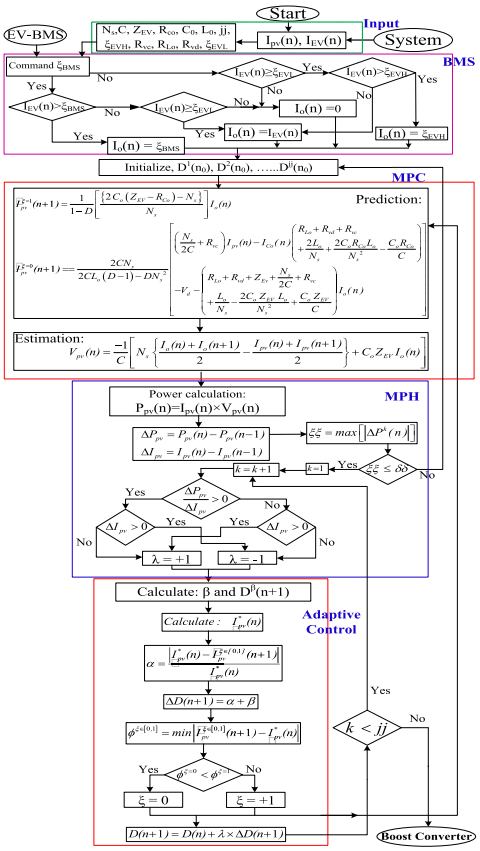

Fig. 5. Flowchart of VSPC for GMPPT and BMS.

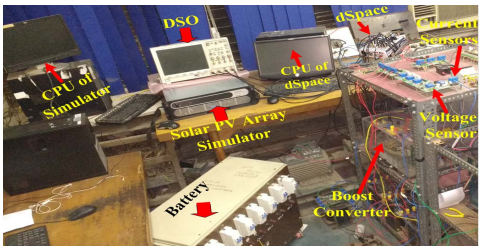

Fig. 6. Photograph of hardware setup.

as well as the waveforms of I_{PV} and V_{PV} show steady-state oscillation, which are the waveforms of the P&O algorithm. In Fig. 7(c) and 8(b), the waveforms of P&O-PSO algorithm reveal that deviation issues are solved, while tracking duration is still high as well as ossifications are available in the waveform of steady-state condition. Therefore, these all issues are resolved in this work, by VSPC, which obtained performances are illustrated in Figs. 7(d) and 8(c).

In this VSPC algorithm, both, oscillations as well as deviations are successfully mitigated. The deviations are eliminated by proper direction selection, which is achieved by the MPC in MPH. Moreover, the oscillations are reduced by an optimal duty cycle selection by adaptive control. Here, in every step, the duty cycle is tuned by adaptive control, and an improvement is calculated as well as information about the next step is predicted by MPC.

Therefore, after 3–4 iterations, the oscillations in the waveforms of V_{PV}, I_{PV}, and P_{PV} are negligible, which is illustrated in Figs. 7(d) and 8(c). Figs. 7(d) and 8(c) reveal that the variations in V_{PV}, I_{PV}, and P_{PV} are in the range of mille, and continually decreasing in nature, which after a few iterations

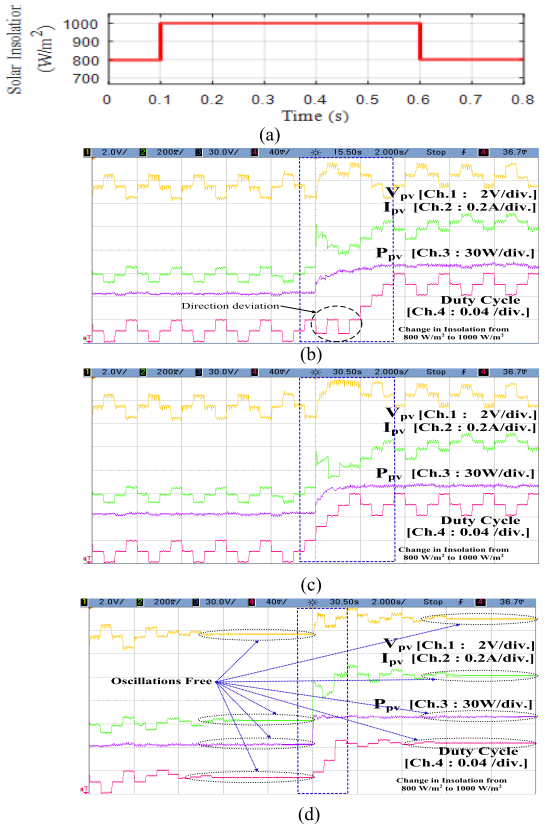

Fig. 7. Experimental results of all algorithms, in sudden irradiation rise condition (uniform shading condition). (a) Pattern of solar irradiation. (b) P&O. (c) P&O-PSO. (d) VSPC.

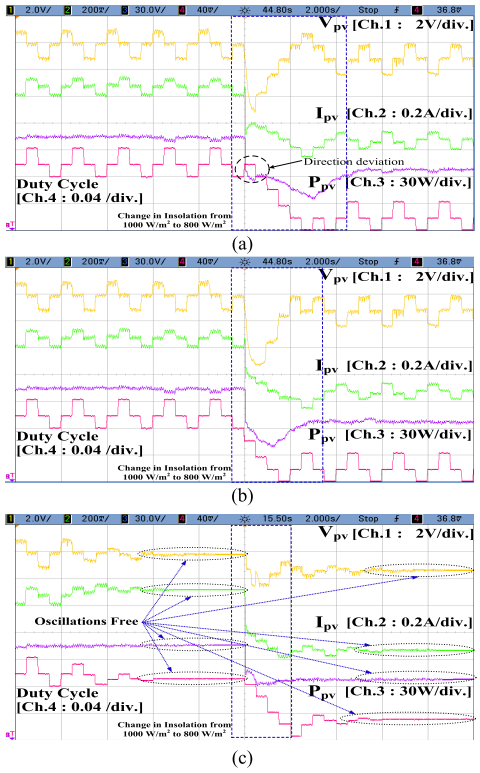

Fig. 8. Experimental results of all algorithms, in sudden irradiation fall condition (uniform shading condition). (a) P&O. (b) MP&O. (c) VSPC.

goes into the range of micro and nano. These performances show negligible or almost zero oscillations in a steady-state condition. Moreover, in the dynamic condition, the expansion

of the duty cycle rapidly reaches the MPP zone, and after reaching the MPP zone, it starts convergence toward the steady state, which is illustrated in Figs. 7(d) and 8(c). This behavior shows a good dynamic performance.

B. Partial Shading Condition on Solar PV Panel

During testing on partially shaded conditions, five types of shading patterns are considered, and corresponding power–voltage (P–V) characteristics are shown in Fig. 9. In this test, $I_{sc} = 40$ A, $V_{oc} = 380$ V, and $V_{EV} = 500$ V are considered. Here, the change of shading pattern is considered every 2 s. The obtained results for P&O-PSO and proposed VSPC are shown in Fig. 10(a) and (b), respectively.

During the partially shaded condition, the P&O algorithm is unable to find the GMPPT [34]. Therefore, P&O is not considered during the partially shaded condition. Here, the most recent technique P&O-PSO [34] is considered for comparative study. The obtained results of P&O-PSO and VSPC techniques for the partially shaded condition are illustrated in Fig. 10(a) and (b), respectively. Here, $\xi_{EVL} = 5$ A, and $\xi_{EVH} = 25$ A are considered. According to different types of shading conditions, the minimum I_{EV} is 8.1 A and the maximum I_{EV} is 19.3 A, which are in between ξ_{EVL} and ξ_{EVH}. Therefore, the BMS of VSPC allows it to operate at GMPP and charges EV with the maximum possible current.

Fig. 10(a) shows that the P&O-PSO is taking an average of 1.7 s to track the global maximum power point (GMPP). In the worst condition, the maximum tracking duration of the P&O-PSO algorithm is 2 s, and in the best condition, the minimum tracking duration of the P&O-PSO algorithm is 1.3 s. In the same situation and same operating condition, the average GMPP tracking duration of the proposed VSPC algorithm is 0.9 s, which is shown in Fig. 10(b). In the worst condition, the maximum tracking duration of the VSPC algorithm is 1 s, and in the best condition, the minimum tracking duration of the VSPC algorithm is 0.5 s. These performances show that in dynamic conditions, the tracking speed of the VSPC algorithm is 47% faster, with respect to the P&O-PSO algorithm.

This marvelous performance of VSPC is due to the MPC and adaptive control. In a steady-state condition, this technique tries to minimize the fitness function, which helps in the estimation of the exact duty cycle. Therefore, the oscillations are negligible in steady-state conditions. In dynamic change conditions, the "MPH" section senses the change and adaptive control explores the duty cycle search behavior. Here 1% power envelop concept is used for condition detection and exploration. This exploration is till the GMPP region. After that, MPC and adaptive control combinedly converge on the true GMPP point. In VSPC, the key to success is these calculations. Because, during dynamics conditions, the exact direction and the suitable updating factor are decided from these calculations, which helps in quick searching. Moreover, during steady-state conditions, the searching converses exponentially, which shorts out the oscillation problem.

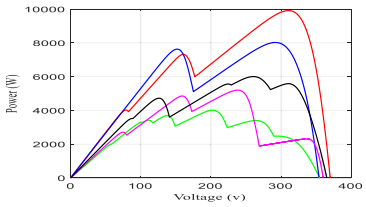

Fig. 9. P–V characteristics of solar PV panel during the partially shading.

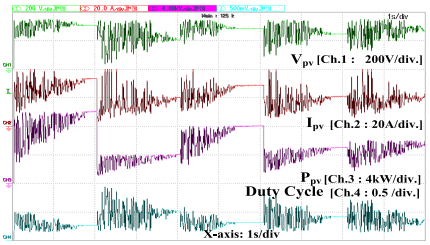

(a)

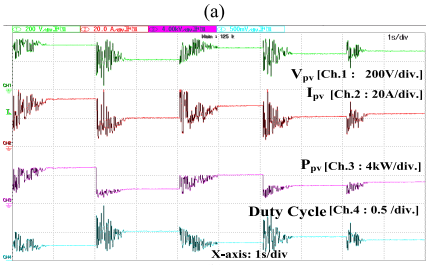

(b)

Fig. 10. Obtained waveforms in partial shading condition by using (a) P&O-PSO and (b) VSPC algorithm.

IV. Stability Analysis

For stability analysis of this VSPC control algorithm, a frequency domain study of Fig. 2(b) is carried out. Out of several methods, in this work, the system stability is analyzed through a Bode plot [23], which requires a state space model of the system.

1) In the "ON" state, the derived state-space model from (4) to (9) is as

$$\begin{bmatrix} \frac{dI_L(t)}{dt} \\ \frac{dV_c(t)}{dt} \\ \frac{dV_{co}(t)}{dt} \end{bmatrix} = \begin{bmatrix} 0 & \frac{1}{L} & 0 \\ \frac{1}{C} & 0 & 0 \\ 0 & 0 & \frac{1}{Z_{EV}C_o} \end{bmatrix} \begin{bmatrix} I_L(t) \\ V_c(t) \\ V_{co}(t) \end{bmatrix} + \begin{bmatrix} 0 \\ \frac{-1}{C} \\ 0 \end{bmatrix} \left[I_{pv}(t) \right] \tag{33}$$

$$V_o = \begin{bmatrix} 0 & 0 & 1 \end{bmatrix} \begin{bmatrix} I_L(t) \\ V_c(t) \\ V_{co}(t) \end{bmatrix}. \tag{34}$$

2) In "OFF" state, the derived state-space model from (10)–(20) is as

$$\begin{bmatrix} \frac{dI_L(t)}{dt} \\ \frac{dV_c(t)}{dt} \\ \frac{dV_{co}(t)}{dt} \end{bmatrix} = \begin{bmatrix} 0 & \frac{1}{L} & \frac{-1}{L} \\ \frac{-1}{C} & 0 & 0 \\ \frac{1}{C_o} & 0 & \frac{-1}{Z_{EV}C_o} \end{bmatrix} \begin{bmatrix} I_L(t) \\ V_c(t) \\ V_{co}(t) \end{bmatrix} + \begin{bmatrix} 0 \\ \frac{1}{C} \\ 0 \end{bmatrix} \left[I_{pv}(t) \right] \tag{35}$$

$$V_o = \begin{bmatrix} 0 & 0 & 1 \end{bmatrix} \begin{bmatrix} I_L(t) \\ V_c(t) \\ V_{co}(t) \end{bmatrix}. \tag{36}$$

TABLE I
PERFORMANCE COMPARISONS OF ALL ALGORITHMS

Algorithm / Parameter	P&O	WODE	P&O-PSO	VSPC
Applicable for uniform shading	Yes	Yes	Yes	Yes
Applicable for partially shading	No	Yes	Yes	Yes
Steady state oscillation	High	Low	Low	Negligible
Power loss (%)	2.7%	1%	0.9%	0.6%
Deviation from track	High	Moderate	Moderate	No
suitability for low-cost microcontroller (Memory)	Yes, 4MB	No, 40MB	No, 37MB	Yes, 5MB
Tracking time during GMPP	-	2.1s	1.7s	0.9s
Efficiency (In steady-state)	97.3%	98.1%	99.1%	99.4%
Efficiency (In dynamic condition)	94.4%	94.9%	98.3%	99.2%
Algorithm complexity (Number of calculations by microcontroller in one sampling period)	4	15	13	7
Overall performance	Poor	Poor	Average	Good
Requirement of Current Sensor	1	1	1	2
Requirement of Voltage Sensor	1	1	1	0
Overall Cost of the Controller	High	Moderate	Moderate	Low
Overall Accuracy	Low	Low	Average	Very High

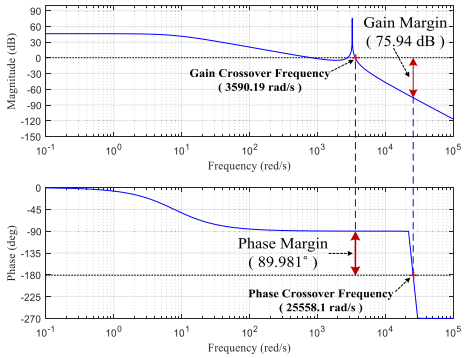

Fig. 11. Bode plot of complete system.

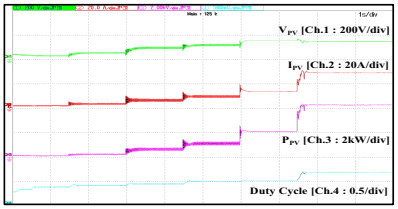

Fig. 12. Waveform of steady-state condition in EN50530 test condition (European condition).

Combining both states, the equivalent state-space model is as

$$\begin{bmatrix} \frac{dI_L(t)}{dt} \\ \frac{dV_c(t)}{dt} \\ \frac{dV_{co}(t)}{dt} \end{bmatrix} = \begin{bmatrix} 0 & \frac{1}{L} & \frac{D-1}{L} \\ \frac{2D-1}{C} & 0 & 0 \\ \frac{1-D}{C_o} & 0 & \frac{2D-1}{Z_{EV}C_o} \end{bmatrix} \begin{bmatrix} I_L(t) \\ V_c(t) \\ V_{co}(t) \end{bmatrix} + \begin{bmatrix} 0 \\ \frac{1-2D}{C} \\ 0 \end{bmatrix} \begin{bmatrix} I_{pv}(t) \end{bmatrix} \quad (37)$$

$$V_o = \begin{bmatrix} 0 & 0 & 1 \end{bmatrix} \begin{bmatrix} I_L(t) \\ V_c(t) \\ V_{co}(t) \end{bmatrix}. \quad (38)$$

The used circuit parameters are, $L = 1.5$ mH, $C = 100$ μF, $C_o = 1000$ μF, $Z_{EV} = 218$ Ω, and $T_s = 10$ kHz. Moreover, duty cycle $(D) = 0.499$. By using these parameters, the derived state space model is as (39) and (40), shown at the top of the next page, where $G(s)$ is the final transfer function.

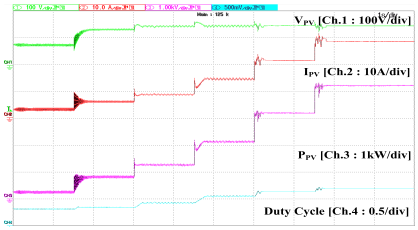

Fig. 13. Waveform of steady state condition in EN50530 test condition (Californian condition).

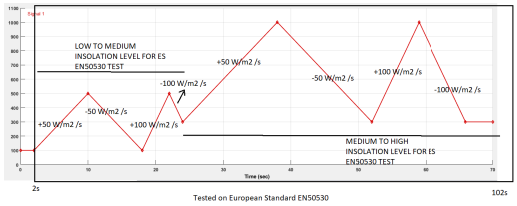

Fig. 14. Waveform of irradiance pattern in EN50530 dynamic efficiency test condition.

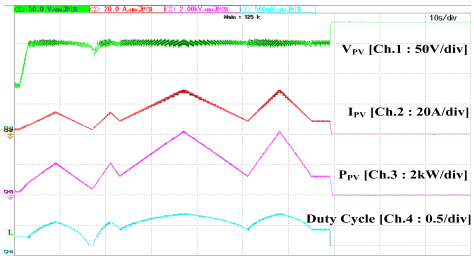

Fig. 15. Waveform of dynamic condition in EN50530 test condition.

Using this $G(s)$, the stability and stability margin are analyzed through a Bode plot. The Bode plot for this proposed system is shown in Fig. 11.

It shows that obtained phase margin and gain margin both are positive, as well as the gain crossover frequency is lower than the phase crossover frequency, which means the system is stable [26]. Because the phase margin measures how much phase variation is needed at the gain crossover frequency to lose stability. Similarly, the gain margin measures what relative gain variation is needed at the gain crossover frequency to lose stability. Together, these two numbers give an estimate of the "safety margin" for closed-loop stability. In this system, the phase margin is 89.981° and the gain margin is 75.94 dB. Moreover, the gain crossover frequency is 3590.19 red/s and phase crossover frequency is 25558.1 red/s. The gap between these two crossover frequencies is very large, which gives an assurance of stability and robustness. The analytical analysis of all MPPT algorithms on different conditions and parameters is given in Table I, which proves that the VSPC MPPT algorithm is very suitable for MPPT.

V. INDUSTRIAL SUITABILITY TEST ON EUROPEAN STANDARD EN50530

To prove the industrial suitability, the developed VSPC technique is tested on European Standard (ES) EN50530 [27]. According to the EN50530 standard, in the first phase, the steady-state efficiencies are calculated on European and Californian benchmark standard efficiency equations. The standard benchmark European and Californian efficiency equations [27]

$$\left.\begin{aligned}\begin{bmatrix}\frac{dI_L(t)}{dt}\\ \frac{dV_c(t)}{dt}\\ \frac{dV_{co}(t)}{dt}\end{bmatrix}&=\begin{bmatrix}0 & 666.67 & -334\\ -20 & 0 & 0\\ 501 & 0 & -9.17\times10^{-3}\end{bmatrix}\begin{bmatrix}I_L(t)\\ V_c(t)\\ V_{co}(t)\end{bmatrix}+\begin{bmatrix}0\\ 20\\ 0\end{bmatrix}\left[I_{pv}(t)\right]\\ V_o&=\begin{bmatrix}0 & 0 & 1\end{bmatrix}\begin{bmatrix}I_L(t)\\ V_c(t)\\ V_{co}(t)\end{bmatrix}\end{aligned}\right\} \tag{39}$$

$$G(s)=\frac{8.265\times10^9}{s^3+8.135\times s^2+1.054\times10^7\times s+8.146\times10^7} \tag{40}$$

are as follows:

$$\xi_{Eu}=\begin{pmatrix}0.03\times\xi_{5\%}+0.06\times\xi_{10\%}+0.13\times\xi_{20\%}\\ +0.10\times\xi_{30\%}+0.48\times\xi_{50\%}+0.20\times\xi_{100\%}\end{pmatrix} \tag{41}$$

$$\xi_{Cl}=\begin{pmatrix}0.04\times\xi_{10\%}+0.05\times\xi_{20\%}+0.12\times\xi_{30\%}\\ +0.21\times\xi_{50\%}+0.53\times\xi_{75\%}+0.05\times\xi_{100\%}\end{pmatrix} \tag{42}$$

where 5%, 10%, 20%, 50%, 75%, and 100% are different solar irradiance levels where the base solar irradiance is 1000 W/m^2. ξ is efficiency at different solar irradiance levels. ξ_{Eu} and ξ_{Cl} are European and Californian efficiency in a steady-state condition, respectively.

The obtained waveforms during the European and Californian efficiency test conditions are shown in Figs. 12 and 13.

In the second phase of the EN50530 standard, the performance of the developed VSPC technique is tested in dynamic conditions [27]. According to EV50530, the two types of dynamic conditions are considered: low to medium insolation (LMI) and medium to high insolation (MHI) levels. During LMI, solar irradiance varies between 100–500 W/m^2, with different slopes in a ramp manner. During MHI, solar irradiance varies between 300–1000 W/m^2, with different slop is in ramp manner [27]. In this situation, the efficiency is calculated using the following equation:

$$\xi_{dy}=\frac{1}{\lambda}\sum_{\upsilon=1}^{\lambda}\frac{\sum_{\upsilon}\text{Extracted}\,P_{PV}}{\sum_{\upsilon}\text{Available}\,P_{PV}} \tag{43}$$

where λ is the total number of sections in different irradiance bands, and ξ_{dy} is efficiency in dynamic conditions.

During the test, the irradiance pattern and obtained results are shown in Figs. 14 and 15, respectively.

From, Figs. 12, 13, and 15, the calculated ξ_{Eu}, ξ_{Cl}, and ξ_{dy} are 99.53%, 99.37%, and 99.21%, respectively. Here the obtained all efficiencies are more than 99%. Therefore, according to the EN50530 standard [27], the maximum power extraction efficiency in each test condition, more than 99% proves the suitability for industrial application. On this basis, the developed VSPC scheme depicts the suitability for real-time application [29], [30].

VI. Conclusion

A new VSPC scheme has been proposed for the MPH to SP-EV charging system. In this control, MPC predicts the system state in the horizon of time, for eliminating the voltage sensor, which reduces the cost of the controller, and enhances the response. Moreover, the adaptive concept has been used for deciding the step size, which accelerates the tracking process and improves dynamic performance during irradiation change as well as reduces the ripples of the power waveform in a steady-state condition. Moreover, the external BMS compatibility and additional battery charging safety support features have been integrated with VSPC. The performance of the VSPC for GMPPT under uniformly shaded and partially shaded conditions has been compared to the performance of the P&O and P&O-PSO techniques in the same irradiance, temperature, shading, and hardware condition. The experimental results of the VSPC show superiority over P&O and P&O-PSO techniques. Moreover, its rapid dynamic performance and smooth steady-state response of the controller show the suitability of the control technique for every sophisticated and critical use, like SP-EV system, satellite, automation industry, robotics, etc.

Acknowledgment

The authors would like to thank the Government of India, for funding this work, through Science and Engineering Research Board (SERB), National Science Chair (NSC) Fellowship.

References

[1] B. Tamimi, C. Canizares, and K. Battacharya, "System stability impact of large-scale and distributed solar photovoltaic generation: The case of Ontario, Canada," *IEEE Trans. Sustain. Energy*, vol. 4, no. 3, pp. 680–688, Jul. 2013.

[2] N. Kumar, B. Singh, B. K. Panigrahi, and L. Xu, "Leaky-least-logarithmic-absolute-difference-based control algorithm and learning-based InC MPPT technique for grid-integrated PV system," *IEEE Trans. Ind. Electron.*, vol. 66, no. 11, pp. 9003–9012, Nov. 2019.

[3] C. Duan et al., "A solar power-assisted battery balancing system for electric vehicles," *IEEE Trans. Transport Electrific.*, vol. 4, no. 2, pp. 432–443, Jun. 2018.

[4] B. Wang, X. Zhang, U. Manandhar, H. B. Gooi, Y. Liu, and X. Tan, "Bidirectional three-level cascaded converter with deadbeat control for Hess in solar-assisted electric vehicles," *IEEE Trans. Transport. Electrific.*, vol. 5, no. 4, pp. 1190–1201, Dec. 2019.

[5] A. K. Singh, A. K. Mishra, K. K. Gupta, P. Bhatnagar, and T. Kim, "An integrated converter with reduced components for electric vehicles utilizing solar and grid power sources," *IEEE Trans. Transport. Electrific.*, vol. 6, no. 2, pp. 439–452, Jun. 2020.

[6] F. Ahmad, M. S. Alam, S. M. Shariff, and M. Krishnamurthy, "A cost-efficient approach to EV charging station integrated community microgrid: A case study of Indian power market," *IEEE Trans. Transport. Electrific.*, vol. 5, no. 1, pp. 200–214, Mar. 2019.

[7] M. H. Mobarak, R. N. Kleiman, and J. Bauman, "Solar-charged electric vehicles: A comprehensive analysis of grid, driver, and environmental benefits," *IEEE Trans. Transport. Electrific.*, vol. 7, no. 2, pp. 579–603, Jun. 2021.

[8] A. Zahedmanesh, K. M. Muttaqi, and D. Sutanto, "A cooperative energy management in a virtual energy hub of an electric transportation system powered by PV generation and energy storage," *IEEE Trans. Transport. Electrific.*, vol. 7, no. 3, pp. 1123–1133, Sep. 2021.

[9] S. S. Satapathy and N. Kumar, "Modulated perturb and observe maximum power point tracking algorithm for solar PV energy conversion system," in *Proc. 3rd Int. Conf. Recent Develop. Control, Autom. Power Eng. (RDCAPE)*, Oct. 2019, pp. 345–350.

[10] L. Cristaldi, M. Faifer, M. Rossi, and S. Toscani, "An improved model-based maximum power point tracker for photovoltaic panels," *IEEE Trans. Instrum. Meas.*, vol. 63, no. 1, pp. 63–71, Jan. 2014.

[11] M. G. Wanzeller, R. N. C. Alves, J. V. da Fonseca Neto, and W. A. dos Santos Fonseca, "Current control loop for tracking of maximum power point supplied for photovoltaic array," *IEEE Trans. Instrum. Meas.*, vol. 53, no. 4, pp. 1304–1310, Aug. 2004.

[12] O. Lopez-Lapena, M. T. Penella, and M. Gasulla, "A closed-loop maximum power point tracker for subwatt photovoltaic panels," *IEEE Trans. Ind. Electron.*, vol. 59, no. 3, pp. 1588–1596, Mar. 2012.

[13] D. T. Thayalan, H.-S. Lee, and J.-H. Park, "Low-cost high-efficiency discrete current sensing method using bypass switch for PV systems," *IEEE Trans. Instrum. Meas.*, vol. 63, no. 4, pp. 769–780, Apr. 2014.

[14] K. Manickavasagam, "Intelligent energy control center for distributed generators using multi-agent system," *IEEE Trans. Power Syst.*, vol. 30, no. 5, pp. 2442–2449, Sep. 2015.

[15] A. El Khateb, N. A. Rahim, J. Selvaraj, and M. N. Uddin, "Fuzzy-logic-controller-based SEPIC converter for maximum power point tracking," *IEEE Trans. Ind. Appl.*, vol. 50, no. 4, pp. 2349–2358, Jul. 2014.

[16] M. Miyatake, M. Veerachary, F. Toriumi, N. Fujii, and H. Ko, "Maximum power point tracking of multiple photovoltaic arrays: A PSO approach," *IEEE Trans. Aerosp. Electron. Syst.*, vol. 47, no. 1, pp. 367–380, Jan. 2011.

[17] N. Kumar, I. Hussain, B. Singh, and B. K. Panigrahi, "MPPT in dynamic condition of partially shaded PV system by using WODE technique," *IEEE Trans. Sustain. Energy*, vol. 8, no. 3, pp. 1204–1214, Jul. 2017.

[18] O. Abdel-Rahim, H. Funato, and J. Haruna, "Novel predictive maximum power point tracking techniques for photovoltaic applications," *J. Power Electron.*, vol. 16, no. 1, pp. 277–286, Jan. 2016.

[19] S. Sajadian, R. Ahmadi, and H. Zargarzadeh, "Extremum seeking-based model predictive MPPT for grid-tied Z-source inverter for photovoltaic systems," *IEEE J. Emerg. Sel. Topics Power Electron.*, vol. 7, no. 1, pp. 216–227, Mar. 2019.

[20] O. Abdel-Rahim and A. University, "A new high gain DC-DC converter with model-predictive-control based MPPT technique for photovoltaic systems," *CPSS Trans. Power Electron. Appl.*, vol. 5, no. 2, pp. 191–200, Jun. 2020.

[21] A. Hussain, H. A. Sher, A. F. Murtaza, and K. Al-Haddad, "A novel sensor-less current technique for photovoltaic system using DC transformer model based model predictive control," *Int. J. Electr. Power Energy Syst.*, vol. 122, Nov. 2020, Art. no. 106165.

[22] A. Hussain, H. A. Sher, A. F. Murtaza, and K. Al-Haddal, "Improved restricted control set model predictive control (iRCS-MPC) based maximum power point tracking of photovoltaic module," *IEEE Access*, vol. 7, pp. 149422–149432, 2019.

[23] A. Hussain, H. A. Sher, A. F. Murtaza, and K. Al-Haddad, "Revised perturb and observe approach for maximum power point tracking of photovoltaic module using finite control set model predictive control," in *Proc. IEEE 28th Int. Symp. Ind. Electron. (ISIE)*, Jun. 2019, pp. 962–967.

[24] LEM. (May 15, 2015). *Datasheet of Voltage Sensor (LV-25) and Current Sensor (LA 55)*. [Online], Available: http://www.lem.com/docs/products/lv_25-p.pdf

[25] N. Kumar, I. Hussain, B. Singh, and B. K. Panigrahi, "Single sensor-based MPPT of partially shaded PV system for battery charging by using Cauchy and Gaussian sine cosine optimization," *IEEE Trans. Energy Convers.*, vol. 32, no. 3, pp. 983–992, Sep. 2017.

[26] R. W. Erickson and D. Maksimovic, *Fundamentals of Power Electronics*. New York, NY, USA: Kluwer, 2001.

[27] H. Abu-Rub, M. Malinowski, and K. Al-Haddad, *Power Electronics for Renewable Energy Systems, Transportation and Industrial Applications*. Hoboken, NJ, USA: Wiley, 2014.

[28] T. M. Apostol, *Multi Variable Calculus and Linear Algebra, With Applications to Differential Equations and Probability*. Hoboken, NJ, USA: Wiley, 1968.

[29] I. J. Nagrath and M. Gopal, *Control Systems Engineering, Control Systems Engineering*. New Delhi, India: New Age International Private Limited, 2009.

[30] N. Kumar, B. Singh, and B. K. Panigrahi, "Takagi–Sugeno–Kang fuzzy model-based self-adaptive maximum power harvesting technique for PV array: Tested on European standard EN50530," in *Proc. 7th Int. Conf. Power Syst. (ICPS)*, Dec. 2017, pp. 640–645.

[31] P. A. A. Honadia, F. I. Barro, and M. Sané, "Performance analysis of a boost converter with components losses," *Energy Power Eng.*, vol. 10, no. 9, pp. 399–413, 2018.

[32] N. Kumar and S. K. Panda, "Smart high power charging networks and optimal control mechanism for electric ships," *IEEE Trans. Ind. Informat.*, early access, Apr. 26, 2022, doi: 10.1109/TII.2022.3170484.

[33] N. Kumar and S. K. Panda, "A multipurpose and power quality improved electric vessels charging station for the seaports," *IEEE Trans. Ind. Informat.*, early access, Apr. 26, 2022, doi: 10.1109/TII.2022.3170424.

[34] S. Figueiredo and R. N. A. L. E. S. Aquino, "Hybrid MPPT technique PSO-P&O applied to photovoltaic systems under uniform and partial shading conditions," *IEEE Latin Amer. Trans.*, vol. 19, no. 10, pp. 1610–1617, Oct. 2021.

Nishant Kumar (Senior Member, IEEE) received the M.Tech. degree (with Gold Medal) in electrical power systems from the National Institute of Technology Durgapur, Durgapur, India, in 2013, and the Ph.D. degree in power systems from the Department of Electrical Engineering, IIT Delhi, New Delhi, India, in 2019.

He joined the National University of Singapore, Singapore, as a Post-Doctoral Researcher, in 2021. He is currently an Assistant Professor with the Department of Electrical Engineering, IIT Jodhpur, Jodhpur, India. His current research interests include intelligent control of distributed generations and microgrids, cyber security for critical infrastructure, electric vehicle charging infrastructure, and application of soft computing techniques to power system planning, operation, and control. He has authored or co-authored more than 60 papers in world-renowned journals and holds ten patents.

Dr. Kumar was a recipient of more than 20 national or international awards such as the IEEE IAS society Best Thesis Award in 2020, IEEE (India Section) Best Volunteer Award in 2020, etc.

Bhim Singh (Fellow, IEEE) received the B.E. degree in electrical from IIT Roorkee, Roorkee, India, in 1977, and the M.Tech. degree in power apparatus and systems and the Ph.D. degree in electrical from IIT Delhi, New Delhi, India, in 1979 and 1983, respectively.

In 1983, he joined the Department of Electrical Engineering, IIT Roorkee, as a Lecturer, where he became a Reader in 1988. In December 1990, he joined the Department of Electrical Engineering, IIT Delhi, as an Assistant Professor, where he became an Associate Professor in 1994 and a Professor in 1997. He was the Head of the Department of Electrical Engineering, IIT Delhi, from July 2014 to August 2016. He was the Dean of Academics with IIT Delhi from August 2016 to August 2019. He has guided 110 Ph.D. dissertations and 177 M.E./M.Tech./M.S.(R) theses. He has filed 103 patents. He has executed 90 sponsored and consultancy projects. His current research interests include solar photovoltaic (PV) grid interfaced systems, microgrids, power quality monitoring and mitigation, solar PV water pumping systems, and improved power quality ac–dc converters.

Dr. Singh was a JC Bose Fellow of DST, Government of India, from December 2015 to June 2021. He has been the CEA Chair Professor from January 2019 to June 2021. He has been the SERB National Science Chair since July 2021.

Bijaya Ketan Panigrahi (Senior Member, IEEE) is currently the Institute Chair Professor with the Department of Electrical Engineering, IIT Delhi, New Delhi, India, where he is also the Head of the Centre for Automotive Research and Tribology (CART). He has authored or co-authored more than 250 research articles in various international and national journals, including IEEE Transactions, Elsevier, Springer, and conferences of international repute. His current research interests include biomedical imaging, machine intelligence, evolutionary computing, and digital signal processing techniques and their application for power quality monitoring and power system protection.

Dr. Ketan Panigrahi has served as an Editorial Board Member and an Associate Editor for different international journals. He is also a fellow of the Indian National Academy of Engineering (INAE). He is also associated with various international conferences in various capacities.